

Properties of solar pores

Peter Sütterlin*

Kiepenheuer-Institut für Sonnenphysik, Schöneckstrasse 6, D-79104 Freiburg, Germany

Received 20 November 1997 / Accepted 19 January 1998

Abstract. We present the results of an extensive investigation of the properties of solar pores. Spectra of all 4 Stokes parameters of several magnetic sensitive absorption lines as well as Stokes I only spectra of lines with low or vanishing Landé-factor have been observed. An inversion code based on the Levenberg-Marquardt algorithm was written, incorporating the full radiative transfer equations. This code adapts a set of parameters that are used to represent the magnetic and thermodynamic state of the atmosphere to best-fit a set of observed line profiles.

The results show that the value of all relevant parameters are intimately related to the size of the pores, therewith confirming the role of solar pores as a link between (bright) magnetic flux tubes and sunspots. In particular the inclination of the magnetic field lines at the outer rim of a pore, which is affected by the vertical field gradient, seems to put an upper limit on the diameter of pores where the inclination reaches a value that might trigger the formation of a penumbra.

Key words: Sun: magnetic fields – sunspots – polarization

1. Introduction

Magnetic field concentrations on the solar surface show up in a variety of sizes, from still hardly resolvable flux tubes up to the sunspots. Pores are located towards the small end of this chain, however at an interesting point. They represent a link between the magnetic knots, which are of average photospheric intensity and have field strengths of some 1500 G, and the sunspots, which have low intensities and much higher field strengths. Many questions still remain: Is there a relation between the size of a pore and its continuum intensity? What are the inclination angles of the magnetic field lines? And, possibly related to the last one, why do sunspots have a penumbra, and pores do not?

To get an answer to those questions, we have to learn more about the internal structure of pores, their atmosphere as well as the geometry of the magnetic field. Unfortunately, their small size of $\leq 4''$ puts high constraints to the seeing conditions as

well as to the data reduction. In particular the correction for stray light, either due to instrumental defects or from photospheric light scattered in by the earth's turbulent atmosphere, plays a crucial role in the correct interpretation of spectroscopic and polarimetric observations. There have been numerous attempts to determine the true intensity contrast of pores: Rossbach & Schröter (1970) used an idealized Point Spread Function (PSF) to deconvolve their observations and find values around 0.1 of the photospheric intensity. A first empiric thermodynamic model (Sütterlin 1991) predicts values rising from 0.2 at 400 nm to 0.46 at 700 nm. Using polarimetric spectra of spectral lines that show a Zeeman-pattern without unshifted π -component, Thim (1993) finds 0.13 at 400 nm and 0.43 at 600 nm. Bonet et al. (1995) use the moon limb during a partial eclipse to correct the atmospheric disturbances. They find an average of 0.46 at 670 nm. The authors also report a clear correlation between the size of a pore and its continuum intensity - a fact already noticed by Loughhead & Bray (1961) from observations of the evolution of a small sunspot group, although without giving any absolute values.

Even less is known about the structure of the magnetic field. The first observations did concentrate on the value of the field strength (Bumba 1967; Beckers & Schröter 1968; Steshenko 1968). They give an average value of 1400 - 1700 G and observe a rapid drop of the field strength at the rim. More recent work favors slightly higher values: Sütterlin (1991) 1860 G, Thim (1993) 1600 - 2100 G, Keppens & Martínez Pillet (1996) 1700 G. For large pores higher values (1900 - 2600 G) are reported than for small ones (Brants & Zwaan 1982). One has to keep in mind that these values are measured in the geometric height where the used spectral lines are formed. Hence, the much higher field strength of 2300 G found by Muglach et al. (1994) using infrared lines at 1.6μ where the continuum originates some 50 km deeper in the atmosphere, allows to estimate the height gradient of the magnetic field strength inside the pores. They report a value of 5 G km^{-1} . Using several visible lines of different formation heights, Thim (1993) finds 3.3 G km^{-1} ; the empirical model of Sütterlin (1991) predicts a gradient of $2\text{-}3 \text{ G km}^{-1}$.

Theoretical models as well as observations show that the diameter of a pore increases with height in the atmosphere (Simon & Weiss 1970; Zirin & Wang 1992; Sütterlin et al. 1996; Kep-

* *Present address:* Universitäts-Sternwarte, Geismarlandstrasse 11, D-37083 Göttingen, Germany

Correspondence to: pit@uni-sw.gwdg.de

Table 1. Used series

Series	Identification	Date	Telescope	Spectral ranges
I	NOAA 7515	30.5.1993	GCT	6259, 6302
II	NOAA 7518	6.7.1993	VTT	4443, 4656, 4912, 4923, 5052
III	—	7.11.1994	GCT	5123, 5380, 5432, 5434, 5576
				6149, 6173

pens & Martínez Pillet 1996). This also enforces a variation of the inclination of the field lines across the pores diameter. For the simple potential field model of Simon & Weiss the inclination reaches 90° at the rim of a pore of 3000 km in diameter. Contrary to that, results of observations with the Advanced Stokes Polarimeter (Keppens & Martínez Pillet 1996) give an average field inclination of 35° for a sample of 51 pores. The inclination in the model of Sütterlin (1991), 60° - 70° , is in accordance with observational results of Thim (1993) and Sütterlin et al. (1994).

It is the aim of this paper to present a consistent model for pores, based on the numerical inversion of a large sample of observed spectral lines (both magnetic sensitive and insensitive), to solve at least some of the abovementioned questions.

2. Observational data

The observations have been carried out at the German observing facilities located at the Observatorio del Teide, Tenerife (Schröter et al. 1985). Three different data sets were taken on May 5th, 1993, hereafter called I, June 6th, 1993 (II) and November 7th 1994 (III), cf. Table 1. Series I and III involved polarimetric observations, for these the almost polarization-free Gregory-Coudé-Telescope (GCT) was used. The Stokes-*I* observations of series II were done at the Vacuum Tower Telescope (VTT), which allows to observe up to four wavelengths simultaneously. Table 2 lists some important parameters for all the observed spectral lines.

The device used for the recording of the polarimetric spectra consists of two birefringent calcite columns, a quarter-wave plate, and a half-wave plate. These can be adjusted so that one of the stokes parameters Q , U or V can be observed simultaneously with Stokes I .

2.1. Data processing

In addition to the standard procedure of subtracting the dark current and flatfielding, the spectra had to be corrected for the influence of instrumental straylight. Especially the spectra taken with polarimeter and/or spectrum cutter suffer heavily from the scattering induced by the numerous optical surfaces. This instrumental straylight can be regarded as undispersed and therefore manifests itself in an additional intensity all over the field of view. Hence it reduces the relative line core intensity and the equivalent width of the line. We used the corrected flatfield images (taken with defocussed telescope at disk center) to measure the equivalent widths of all lines used and compared them to the spectra of the Liège Atlas (Delbouille et al. 1973). From the difference we computed the amount of straylight and subtracted it from the observed spectra.

Table 2. Spectral lines used in this work. For each line, central wavelength, Element and ionisation level, excitation energy, effective g -value and equivalent width are given. Following Moore et al. (1966), the letters after the equivalent width show the behavior of the line in sunspot atmospheres.

λ [Å]	El.Ion	χ^l [eV]	g_{eff}	W_λ
4442.835	Fe I	2.17	1.00	57s
4442.994	Zr II	1.48	0.94	26u
4443.201	Fe I	2.86	0.50	95u
4656.978	Fe II	2.88	1.69	27w
4657.204	Ti II	1.24	0.57	38w
4912.022	Ni I	3.77	0.00	47u
4923.933	Fe II	2.89	1.94	167w
5051.513	Ni I	3.64	1.12	47u
5051.643	Fe I	0.91	1.30	111s
5051.900	Cr I	0.94	2.00	20s
5052.147	C I	7.68	1.00	40o
5123.462	Cr I	1.03	0.87	17S
5123.730	Fe I	1.01	0.00	101s
5379.580	Fe I	3.68	1.00	56s
5380.322	C I	7.68	1.00	26N
5432.953	Fe I	4.43	0.67	72s
5434.534	Fe I	1.01	0.00	184S
5576.099	Fe I	3.42	0.00	113u
6149.249	Fe II	3.89	1.33	35W
6151.624	Fe I	2.17	1.83	41s
6173.341	Fe I	2.22	2.50	50u
6175.122	Fe II	6.20	1.24	3s
6175.369	Ni I	4.07	1.25	36w
6259.590	Ni I	4.07	1.50	14w
6302.499	Fe I	3.69	2.50	83w

To get hand on the Stokes V , Q and U information, the two images split by the polarimeter calcites have to be subtracted. It is therefore very important to have the spectral and spatial directions in both spectra perfectly aligned. One has also to check if the image scale in both spectra is exactly the same, as the different optical paths in the spectrograph might cause distortions. All these facts were checked, again using the flatfield spectra, and necessary corrections were applied to all spectra.

3. The inversion code

When speaking of an inversion code, one has to keep in mind that a real inversion, i.e. solving the radiative transfer equations for the model atmosphere with the spectral profile as input, is not possible. Therefore, one has to take the indirect way and adopt a first model, compute the line profiles for that model, compare these line profiles with the observed ones and then change the first model accordingly. Unfortunately, ‘accordingly’

is not obvious, and a lot of trial-and-error is necessary to get to good results. The standard way to ease the procedure is to automate the whole process using a (nonlinear) fit algorithm. For the work presented here, we choose the Levenberg-Marquardt method (see e.g. Press et al. 1988). It combines fast convergence with robustness and is quite easy to implement.

3.1. Parametrisation

The crucial part of a numerical inversion code is the parametrisation of the model so that the code can adapt an atmosphere to reproduce the observed profiles: There have to be enough free parameters as not to restrict the possible results, on the other hand there mustn't be too many of them, as dependent parameters tend to keep the code from converging towards a stable result.

We choose a set of eleven parameters for the representation of the emergent intensity,

$$I(\lambda) = I(\lambda; T_{\min}, T_{\text{dif}}, T_{\text{sl}}, P_{\text{G}}^0, B, dB, \theta, \phi, \xi_{\text{mic}}, v_{\text{b}}, \alpha), \quad (1)$$

where I denotes the Stokes vector $I = (I, Q, U, V)$.

3.1.1. $T_{\min}, T_{\text{dif}}, T_{\text{sl}}$

These parameters describe the change of the temperature with height. A common way has been to use a single parameter to scale a given stratification based on the effective temperature. This way, continuum intensities can be reproduced nicely, however the method fails to adapt to different temperature gradients, needed to give correct line profiles. More realistic is the approach to interpolate between two (or more) given models, based on the temperature in a given height (Emonet 1992). But again, for *one* value of the temperature there is only *one* value of the gradient.

To avoid these problems we have chosen three parameters. We start with the photospheric temperature stratification T_{n}^{\odot} over a range of 1000 km, normalized to vary from 0 to 1. A first temperature run can then be computed as

$$T(h) = T_{\min} + T_{\text{dif}} \cdot T_{\text{n}}^{\odot}(h). \quad (2)$$

Here, T_{\min} is the temperature at the temperature minimum, and T_{dif} is the temperature difference between the minimum and the hottest point. An additional influence to the temperature gradient is introduced by the parameter T_{sl} :

$$T_{\text{n}}^{\odot} \longrightarrow T_{\text{n}}^{\odot}(1 - T_{\text{sl}}(1 - F)), \quad (3)$$

where F is a suitable chosen function that smoothly varies the gradient of the temperature run. Fig. 1 shows an example which also points out that temperature stratifications for different parameter sets may even cross each other.

3.1.2. P_{G}^0

We assume hydrostatic equilibrium for the pore. In this case, for a given temperature run the pressure stratification is already

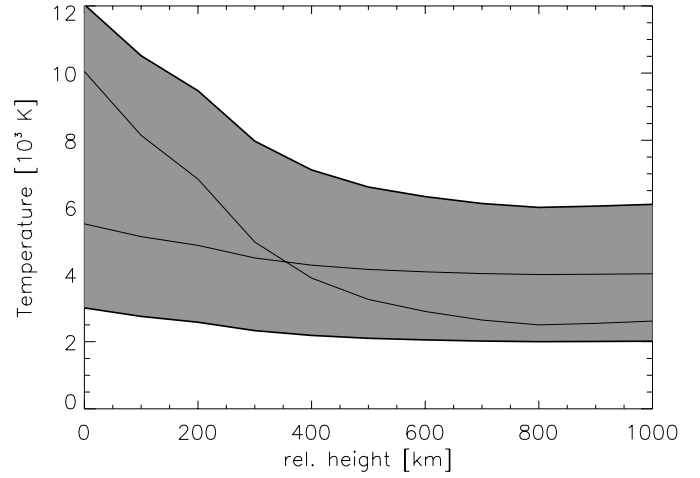


Fig. 1. This plot shows the possible temperature range together with exemplary temperature runs for two different parameter combinations (cf. text).

determined by the pressure in one geometrical height. We arbitrarily choose the pressure at the deepest point as 4th parameter. Also needed for the computation of the gas pressure in each height is the partial pressure of the electrons, P_e . For a given chemical composition, it only depends on temperature and gas pressure, so we could use a precomputed table to interpolate the needed values. Now everything is there to compute the opacities, taking into account the relevant processes, and finally determine the τ -scale.

3.1.3. B, dB, θ, ϕ

These parameters determine the geometry of the magnetic field. Inclination θ and azimuth ϕ of the field are assumed to be independent of height. B is the absolute value of the field strength at the optical depth $\tau_{5000} = 1$ and dB is the (linear) increase of B per $\log \tau = 0.1$.

3.1.4. $\xi_{\text{mic}}, v_{\text{b}}$

Shape and position of a line profile can be influenced by three types of velocities: bulk, micro and macro velocity. As we assume the pore to be a monolithic object, there is no justification for a macroturbulent velocity caused by an unresolved velocity structure. Therefore only microturbulent (ξ_{mic}) and bulk velocity (v_{b}) are considered.

3.1.5. α

The last parameter, α , is commonly called the filling factor. Due to the disturbing influence of the earth's atmosphere, the light observed in the pore is a mixture of the true intensity emitted and the straylight from the surrounding photosphere,

$$I(\lambda) = \alpha I^{\text{pore}} + (1 - \alpha) I^{\odot}. \quad (4)$$

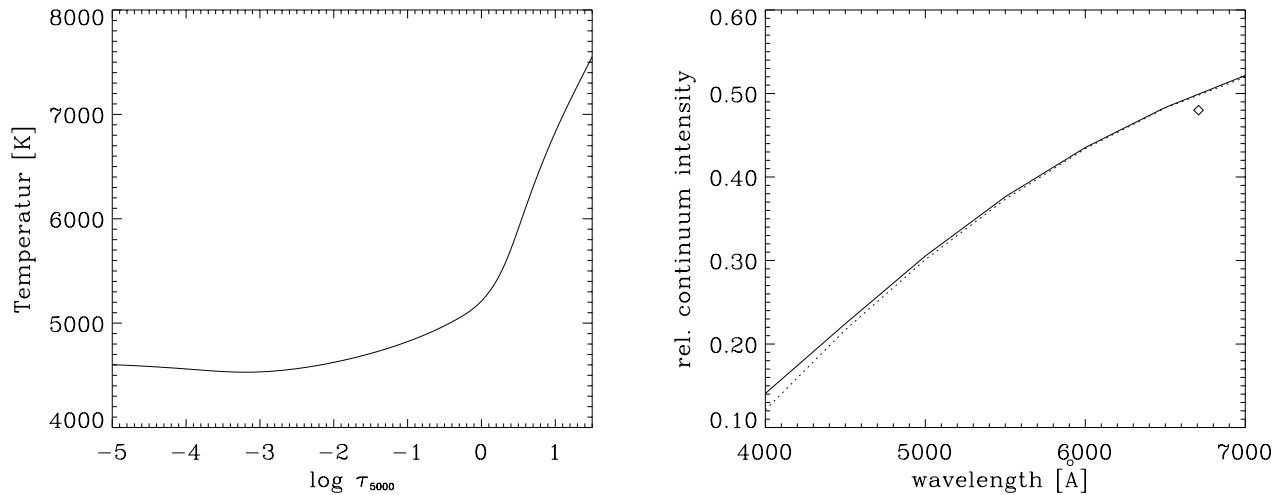


Fig. 2. *Left:* Temperature stratification for pore II. *Right:* Corresponding wavelength dependence of the relative continuum intensity in units of the average quiet photosphere. The dotted curve gives the results of Thim (1993), the diamond marks the value observed by Bonet et al. (1995).

For each line under study, a parameter α is added. The different values of α can be forced to be identical (for simultaneous observations in the same wavelength region), kept in a fixed ratio (simultaneous observations in different wavelength regions), or can be independent of each other (non-simultaneous observations).

3.2. Atomic parameters

In addition to the knowledge of the thermodynamic circumstances, one also has to know the properties of the atomic transition responsible for the investigated spectral line. While most of them are well-known, values for the oscillator strength f and the van der Waals interaction constant C_6 are often hard to find. Hence, we decided to use empirically self-determined values for these two parameters. We used the atmosphere model of Spruit (1981) to compute quiet sun profiles of the lines and changed the two parameters, again using the Levenberg-Marquardt algorithm, so that we were able to reproduce the averaged disc center profiles of a spectral atlas (Delbouille et al. 1973).

3.3. Tests of the code

Several tests have been carried out using the Sunspot Sunspot Model (Avrett 1981) with different geometries of the magnetic field. Various levels of photospheric straylight as well as artificial noise have been added to resemble realistic observations.

In all cases the determined temperature and pressure stratification closely follows the original models. The amount of false light in the data was always correctly detected. The magnetic field strength was within some percent of the true value. Inclination and azimuth of the field were within a $\pm 2^\circ$ range. Only the determination of the gradient in field strength was somewhat problematic. With only one line it was impossible to get reasonable results. Only when at least two spectral lines of different height of formation were used, the value of the gradient was found with less than 20% of error.

Table 3. Apparent diameter and true continuum contrast at 600 nm for the three pores.

No.	\odot	I_{600}
I	4''5	31%
II	3''	43%
III	2''	53%

4. Results

4.1. Continuum intensity

The results (Tab. 3) confirm the earlier findings that the true continuum intensity of a pore is closely related to its size, with small pores being brighter than larger ones.

The most reliable results for the wavelength dependence of the true continuum intensity are based on the inversion of series II. The large number of lines spanning a range of more than 110 nm represents a very sensitive diagnostic tool. As already mentioned, not all lines were observed simultaneously. Consequently, the parameters for the filling factor, α , were divided into three groups, each group containing the α -values for the lines that were observed together. Within each group, the filling factors were kept in a fixed ratio to resemble the influence of the wavelength dependence of the atmospheric distortions. So in fact the inversion code had three parameters to work with.

Fig. 2 shows the temperature stratification and the resulting true continuum intensity in units of the average photospheric intensity.

4.2. Spatial variations

The spectra of the pores have been divided into subfields, each covering approx. $0''.6$, thereby enabling us to investigate variations of all parameters across the pore. Especially in the case of the temperature this provides important information. Up to now, most authors adopted the pore to have a uniform atmosphere,

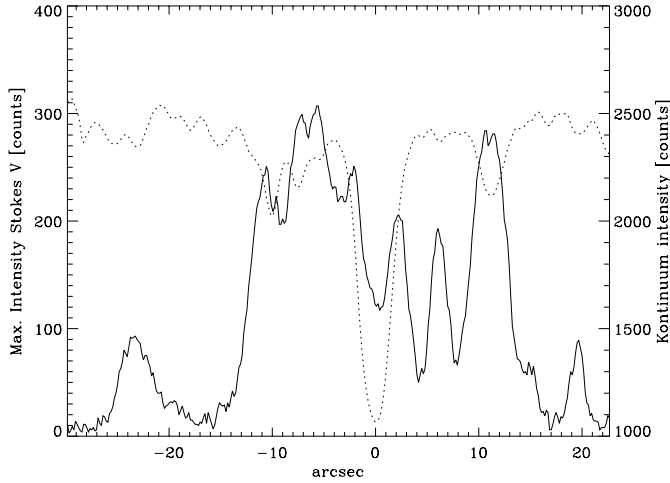


Fig. 3. Unnormalized spatial variation of Stokes- V (solid) and Stokes- I (dotted) for the pore of series I. The observed maxima at the rim of the pore point towards a non-homogeneous temperature structure of the pore.

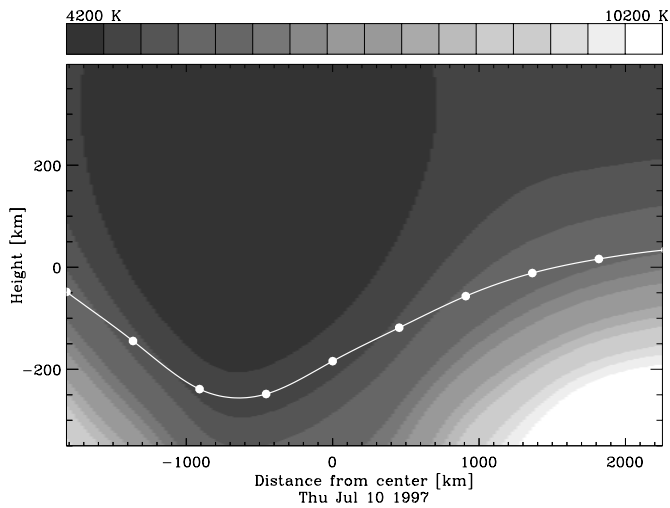


Fig. 4. Two-dimensional temperature structure of the pore. The solid line marks the point where the optical depth τ reaches unity.

the observed variations in intensity stemming only from the different amounts of photospheric straylight. However, already a close look at the Stokes- V intensities shows that this can't be true: Fig. 3 shows the absolute (i.e. not normalized to the local continuum) maximum Stokes- V intensity of pore I. One can clearly see that the intensity has a maximum at the rim of the pore. The Stokes- V amplitude, however, is only dependent on two factors: inclination of the field lines and (local) continuum intensity. As the Stokes- V amplitude drops with growing angle between line of sight (LOS) and field, explaining the observed variation with changes in inclination would imply a more vertical field at the outer boundary of the pore, which is very unlikely. Hence, we have to take the intensity variations as real. This is in accordance with theoretical models of small fluxtubes (Spruit 1981, Steiner 1994). They show that a strong heating occurs along the circumference of the tube due to radiation from the

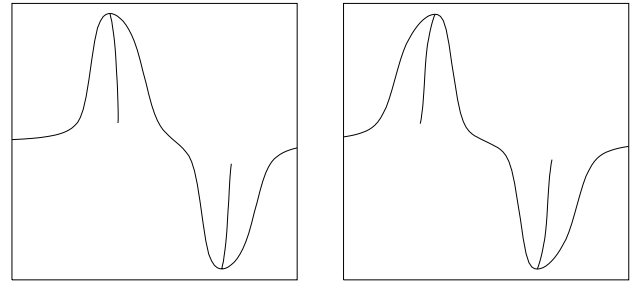


Fig. 5. Influence of a gradient in bulk velocity (left) and field strength (right) on shape and bisector of the Stokes- V profile.

surrounding photosphere. This way, small tubes get up to 30% brighter than the surrounding photosphere (Keller 1992). For larger objects, the radiative cooling (proportional to the area of the structure) overbalances the heating (proportional to the perimeter) and the structure gets dark. But still, the heating occurs and the outer parts should be brighter.

The variation in temperature of course affects the location of the point where optical depth $\tau = 1$ is reached, as is shown in Fig. 4. As this is the reference level for most measurements, the variation has consequences for the other results.

4.3. Magnetic field strength

The magnetic field strength at $\log \tau = -1.5$, the approximate formation height of the Stokes- V maximum, is 2180 G in the center for pore I and 1800 G for pore III, thereby pointing out the correlation between diameter of the pore and maximum field strength already found by Brants & Zwaan (1982).

The magnetic field strength drops to values around 1000 G at the rim of the pore. However, one has to keep in mind that this is not the change within one geometrical height. As shown in the previous section, the reference height $\tau = 1$ changes across the pore, so the values of the field strength are mainly a measurement in different heights in the atmosphere. In fact, they can be explained by the effects of a vertical field gradient alone (see below). This would imply a constant value of the field strength within one geometrical height.

4.4. Vertical field gradient

The inversion code gives an average value of 4.6 G km^{-1} for the vertical field gradient. As this parameter is affected with a large error, we give some additional arguments to fix this value:

4.4.1. Shape of the Stokes- V profile

In general, solar absorption lines are asymmetric. This asymmetry is often measured by means of the line bisector. For a homogeneous object like a pore, an asymmetry may be caused by two reasons: a variation in bulk velocity with height or a vertical field gradient. Fortunately, both effects are easy to separate, as the inclination of the bisectors in the two parts of Stokes- V is

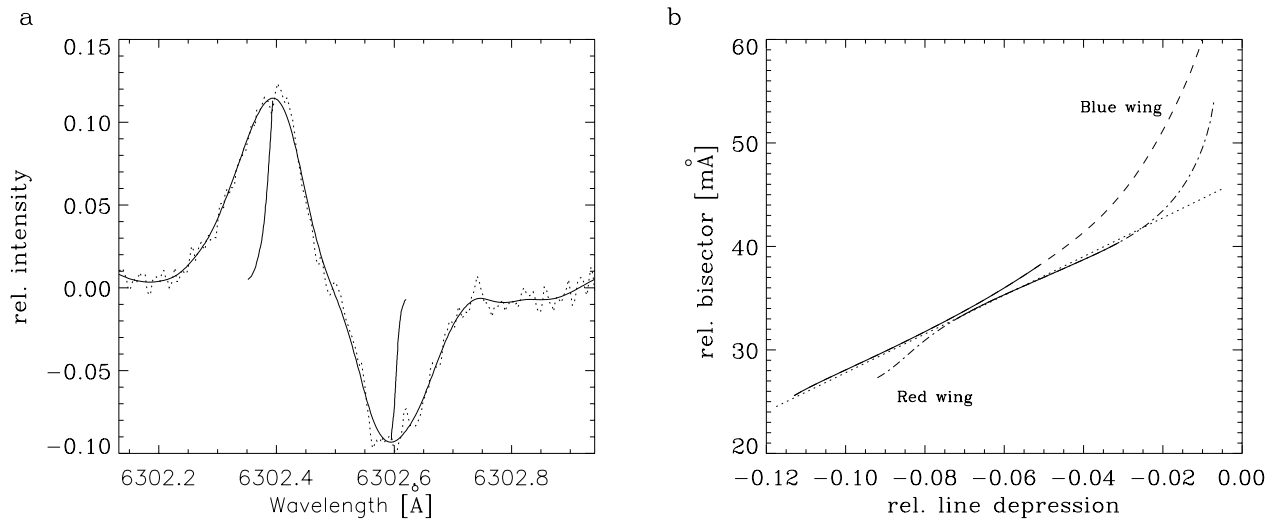


Fig. 6. **a** Observed line asymmetry of Fe I 6302 for series I. **b** Comparison of the bisectors for the red and blue component. The obvious parallelism shows that the asymmetry is dominated by a gradient in magnetic field strength.

parallel for the field gradient case and mirrored for the velocity case (Fig. 5).

A glimpse at the measured Stokes- V profiles (Fig. 6) shows parallel bisectors. This indicates that the asymmetry is predominantly caused by a vertical field gradient. The extrapolated shift between continuum and line core amounts to $20 \text{ m}\text{\AA}$. Together with the height of formation of the line for the maximum of Stokes- V , 100 km , this yields a gradient of 3.9 G km^{-1} . When comparing the slope of both bisectors (Fig. 6 b) one can even confine the maximum value of a velocity gradient. For the shown example, this is less than 180 m s^{-1} over the given range.

4.4.2. Pressure equilibrium

The relative long lifetime of pores (several hours up to days) shows that they are in horizontal pressure equilibrium with the surrounding photosphere. Given a photospheric model, one can compute the maximum field strength within each height and therewith the maximum gradient. With the used model of Vernazza et al. (1976) this estimate confines the field gradient to less than $5\text{--}6 \text{ G km}^{-1}$.

4.4.3. Variation of fieldstrength across the pore

The results have shown that the temperature stratification and therewith the Wilson depression (geometrical depth of $\tau = 1$) change across the pore. What we did was to compute the (relative) formation height of the Stokes- V maximum for each position and then put those together in an absolute frame by using the Wilson depressions. That way, if one plots the differences in field strength versus difference in height, we get an almost linear decay with $3\text{--}4 \text{ G km}^{-1}$ (Fig. 7). This puts an upper limit to the real field gradient, as a larger value would imply an increase of field strength towards the outer parts of the pore which again is very unlikely.

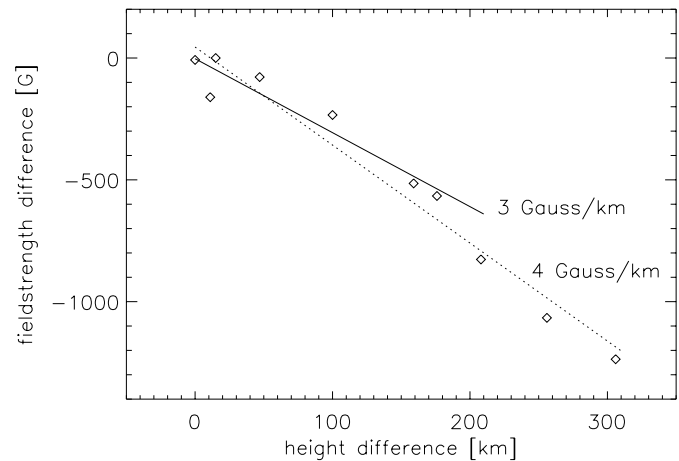


Fig. 7. Scatter plot of differences in measured field strength vs. differences in height of formation for pore I. Depending on the number of included points, the slope is between 3 and 4 Gauss per kilometer.

These facts together confirm that the vertical field gradient in solar pores is approx. 4 G km^{-1} . This is also the upper limit given by the estimate using the observed horizontal variation of field strength and thereby implies that there is no change of the magnetic field strength within one geometrical height.

4.5. Field geometry

Although the tests did show a good accuracy for the results concerning the field geometry, the code had some problems with the real data. The main reason for that was the time delay between the recording of the different Stokes parameters. Especially the linear components Q and U are extremely sensitive to changes in the observing conditions, a slit displacement of only one slit width ($0''.5$) may change the signal as much as 40%. Therefore we choose to use only the Q profile together with V and I for the inversion. For both pores, the field lines are vertical in the

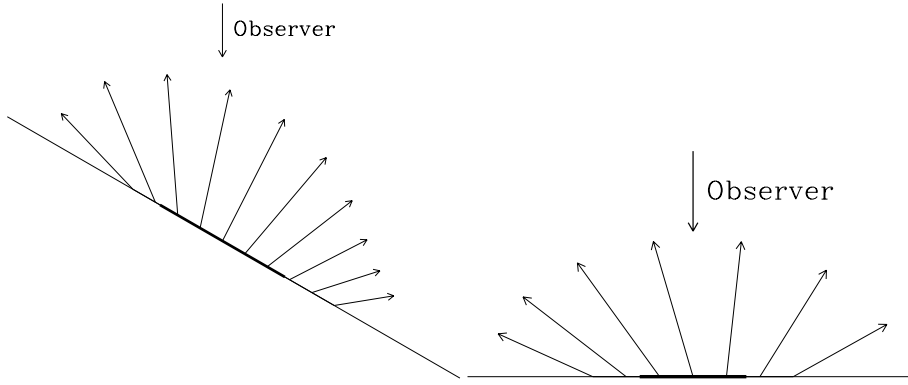


Fig. 8. Inclination angles of the magnetic field for the pores I (left) and III (right). The thick line marks the ‘visible diameter’ of the pore as given by the 90% level in continuum intensity.

Table 4. Spatial variation of the inclination angle γ in degrees for the pores of series I and III (positions in arc seconds).

Δ	-2.5	-1.9	-1.3	-0.6	0.0	0.6	1.3	1.9	2.5	3.1
I	46	16	12	18	23	36	56	65	73	78
III	–	65	51	37	21	5	43	55	–	–

center of the pore, and the inclination with respect to the surface normal reaches 60° at the rim. Table 4 gives the resulting inclination angles with respect to the line of sight, Fig. 8 shows them in graphical form. The asymmetry in the field configuration clearly visible for pore I is most probably caused by the fact that the pore was part of a bipolar group, and the asymmetry in fact points towards the center of the group.

After transformation into the local coordinate system the azimuth angles switch from 0° to 180° at the center of the pore. This indicates that the pore had been cut through the true center in both cases.

5. Discussion

A comparison of the temperature stratification in the center for all three pores with the photospheric temperature run (Fig. 9) shows that the difference between pore and surrounding drops with growing height or — in case of the small pore — even reverses. This has consequences for the center to limb variation (CLV) of pores. With increasing angle between LOS and local surface normal the observed radiation originates in higher levels. As the temperature difference lowers, the relative continuum intensity of pores should drop towards the limb, small ones should even get brighter than the ambient photosphere.

Unfortunately it is impossible to observe the CLV of one particular pore due to the small lifetimes of typical pores. However, a statistical approach shows exactly the predicted behaviour: Keppens & Martínez Pillet (1996) report that they could observe pores only in disk center ($\cos \theta > 0.4$).

The results for the field inclination, on the other hand, are in strong contradiction to the results of Keppens & Martínez Pillet (1996). Using observations made with the Advanced Stokes Polarimeter (ASP) at Sacramento Peak Observatory, they find inclinations of only 30° at the rim of the pore. It is not clear

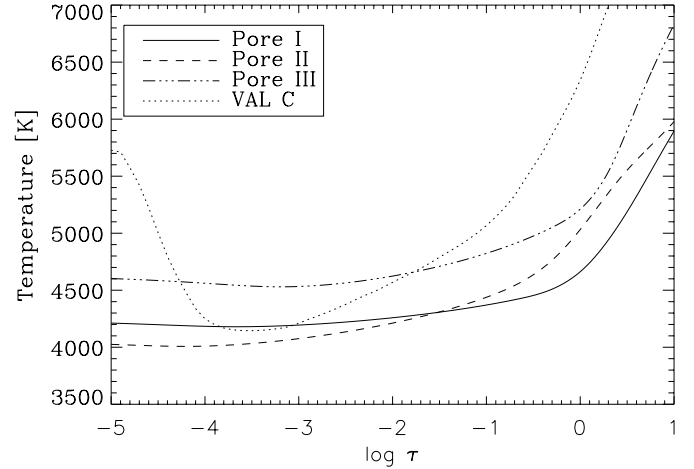


Fig. 9. Comparison of the temperature stratifications at center for all three pores with the photospheric model of Vernazza et al. (1976).

whether these different results are caused by the simpler model of the thermodynamics used for the reduction of the ASP-Data.

Therefore we perform a simple estimate based on the observed vertical field gradient and the conservation of flux. Within each height level, the magnetic flux is given by

$$\Phi = \int_A \mathbf{B} \cdot d\mathbf{a} = \int_0^{2\pi} \int_0^{R(h)} B(r) \cos \gamma(r) dr r d\varphi. \quad (5)$$

As we have seen, the value of the magnetic field strength is constant at a given height. For simplicity, we adopt a linear increase of the inclination angle starting with 0° in the center up to a (height dependent) maximum value at the rim,

$$\gamma(r) = \frac{\gamma_m(h)}{R} r. \quad (6)$$

Now we get the magnetic flux as

$$\Phi(h) = 2\pi B(h) \int_0^{R(h)} r \cos\left(\frac{\gamma_m(h)}{R(h)} r\right) dr, \quad (7)$$

or, after integration,

$$\begin{aligned}\Phi(h) &= \pi BR^2(h) \\ &\left[\frac{2}{\gamma_m(h)} (\cos \gamma_m(h) + \gamma_m(h) \sin \gamma_m(h) - 1) \right] \\ &=: \pi BR^2(h) L(\gamma_m(h))\end{aligned}\quad (8)$$

The conservation of flux, $\Phi(h) = \text{const.}$, now provides us with a simple form for the relative change of the radius. The field line inclination at the rim of the pore is given by

$$\tan \gamma_m(h) = \frac{dR}{dh}.\quad (9)$$

As both L and the field strength depend on height, we get

$$\begin{aligned}\frac{dR}{dh} &= -\frac{1}{2}R(0) \sqrt{\frac{B(0)}{B^3(h)}} \sqrt{\frac{L(\gamma_m(0))}{L^3(\gamma_m(h))}} \\ &\left(\frac{dB}{dh} L(\gamma_m(h)) + B(h) \frac{dL}{d\gamma_m} \frac{d\gamma_m}{dh} \right).\end{aligned}\quad (10)$$

Now we have to find a lower limit for this expression. A closer look at the function $L(\gamma)$ shows that for angles smaller than 80° the following estimates are valid: $0.5 < L < 1.0$ and $|dL/d\gamma| < 10^{-2}$. We can neglect the right term in the last brace which contains the derivatives of L and γ : For the derivative of the maximum inclination angle we can assume that it is smaller than 90° over a typical height scale, e.g. the pressure scale height, and therefore is of the order of 10^{-2} . Hence, the whole expression is of the order $10^3 \cdot 10^{-2} \cdot 10^{-2} = 10^{-1}$. This can be neglected as both parts of the first term are of order 10^0 . As L is monotonically decreasing, the remaining term containing the function L is always larger than one. So we finally find

$$\frac{dR}{dh} > -\frac{R(0)}{2} \sqrt{\frac{B(0)}{B^3(h)}} \frac{dB}{dh}.\quad (11)$$

For a typical pore (diameter $3'' \equiv 2150$ km, $B(h) = 2150$ G, field gradient -4 Gkm $^{-1}$ and $dh = 100$ km) this yields as a lower limit for the inclination angle at the outer rim

$$\gamma_m > 48^\circ\quad (12)$$

in accordance to the results presented in this paper.

Acknowledgements. I wish to thank E.H. Schröter for initiating this work and for many years of support and fruitful discussion.

The VTT and the GCT are operated on the island Tenerife by the Kiepenheuer-Institut and the Universitäts-Sternwarte Göttingen in the Spanish Observatorio del Teide of the Instituto de Astrofísica de Canarias.

References

- Avrett E.H., 1981, in: Cram L.E., Thomas J.H. (eds.) *The Physics of Sunspots*, Sacramento Peak Observatory, Sunspot
 Beckers J.M., Schröter E.H., 1968, *Sol. Phys.* 4, 142
 Bonet J.A., Sobotka M., V zquez M., 1995 *A&A* 296, 241

- Brants J.J., Zwaan C., 1982, *Sol. Phys.* 80, 251
 Bumba V., 1967, *Sol. Phys.* 1, 371
 Delbouille L., Neven L., Roland G., 1973, *Photometric Atlas of the Solar Spectrum from 3000Å to 10000Å*, Institut d'Astrophysique de l'Université de Liège
 Emonet T., 1992, Thesis, ETH Zürich
 Keller C.U., 1992, *Nature* 359, 307
 Keppens R., Martínez Pillet V., 1996, *A&A* 319, 229
 Loughhead R.E., Bray R.J., 1961, *Aust. J. Phys.* 14, 347
 Moore C.E., Minnaert M.G.J., Houtgast J., 1966, *NBS Monograph* 61
 Muglach K., Solanki S.K., Livingston W.C., 1994, In: Rutten R.J., Schrijver C.J. (eds.) *Solar Surface Magnetism*, Kluwer
 Press W.H., Flannery B.P., Teukolsky S.A., Vetterling W.T., 1988, *Numerical Recipes*, Cambridge University Press, Cambridge
 Rossbach M., Schröter E.H., 1970, *Sol. Phys.* 12, 95
 Schröter E.H., Soltau D., Wiehr E., 1985, *Vistas Astron.* 28, 519
 Simon G.W., Weiss N.O., 1970, *Sol. Phys.* 13, 85
 Spruit H., 1981, In: Jordan S. (ed.) *The Sun as a Star*, NASA SP-450
 Steiner O., 1994, In: Rabin D.M., Jefferies J. (eds.) *Infrared Solar Physics*, Kluwer
 Steshenko N.V., 1968, In: Kiepenheuer K.O. (ed.) *Structure and Development of Solar Active Regions*, Reidel, IAU Symp. 35
 Sütterlin P., 1991, Diplomarbeit, Universität Freiburg
 Sütterlin P., Thim F., Schröter E.H., 1994, In: Schüssler M., Schmidt W. (eds.) *Solar Magnetic Fields*, Cambridge University Press, p. 213
 Sütterlin P., Schröter E.H., Muglach K., 1996, *Solar Phys.* 164, 311
 Thim F., 1993, Diplomarbeit, Universität Freiburg
 Vernazza J.E., Avrett E.H., Loeser R., 1976, *ApJS* 30, 1
 Zirin H., Wang H., 1992, *ApJ* 385, L27